Ultrafine-scale magnetostratigraphy of marine ferromanganese crust

Hirokuni Oda[1], Akira Usui[2], Isoji Miyagi[1], Masato Joshima[1], Benjamin P. Weiss[3], Chris Shantz[3], Luis E. Fong[4], Krista K. McBride[4], Rene Harder[4], and Franz J. Baudenbacher[4]

[1]*Geological Survey of Japan, AIST (National Institute of Advanced Industrial Science and Technology), Central 7, 1-1-1 Higashi, Tsukuba 305-8567, Japan*

[2]*Kochi University, 2-5-1 Akebono, Kochi 780-8520, Japan*

[3]*Massachusetts Institute of Technology, 77 Massachusetts Avenue, Cambridge, Massachusetts 02139, USA*

[4]*Vanderbilt University, 2201 West End Avenue, Nashville, Tennessee 37235, USA*

ABSTRACT

Hydrogenetic ferromanganese crusts are iron-manganese oxide chemical precipitates on the seafloor that grow over periods of tens of millions of years. Their secular records of chemical, mineralogical, and textural variations are archives of deep-sea environmental changes. However, environmental reconstruction requires reliable high-resolution age dating. Earlier chronological methods using radiochemical and stable isotopes provided age models for ferromanganese crusts, but have limitations on the millimeter scale. For example, the reliability of $^{10}Be/^{9}Be$ chronometry, commonly considered the most reliable technique, depends on the assumption that the production and preservation of ^{10}Be are constant, and requires accurate knowledge of the ^{10}Be half-life. To overcome these limitations, we applied an alternative chronometric technique,

magnetostratigraphy, to a 50-mm-thick hydrogenetic ferromanganese crust (D96-m4) from the northwest Pacific. Submillimeter-scale magnetic stripes originating from approximately oppositely magnetized regions oriented parallel to bedding were clearly recognized on thin sections of the crust using a high-resolution magnetometry technique called scanning SQUID (superconducting quantum interference device) microscopy. By correlating the boundaries of the magnetic stripes with known geomagnetic reversals, we determined an average growth rate of 5.1 ± 0.2 mm/m.y., which is within 16% of that deduced from $^{10}Be/^{9}Be$ method (6.0 ± 0.2 mm/m.y.). This is the finest-scale magnetostratigraphic study of a geologic sample to date. Ultrafine-scale magnetostratigraphy using SQUID microscopy is a powerful new chronological tool for estimating ages and growth rates for hydrogenetic ferromanganese crusts. It provides chronological constraints with the accuracy promised by the astronomically calibrated magnetostratigraphic time scale (1–40 k.y.).

INTRODUCTION

Hydrogenetic ferromanganese crusts are typically formed through accumulation of colloidal precipitates of iron-manganese oxide on seamounts away from terrigenous sources, where sedimentation is scarce. Due to their continuous slow growth rate (1–10 mm/m.y.), hydrogenetic ferromanganese crusts record long-term environmental variations, including bottom-water circulation patterns (van de Flierdt et al., 2004) and supply of dust and sediments from continents (Banakar et al., 2003). The crusts also record extraterrestrial events such as meteoroid impacts (Prasad, 1994).

In order to reconstruct geological and oceanographic signatures from ferromanganese crusts, it is crucial to provide a reliable fine-scale age model for each

46 crust. A first-order age model was established by dividing the thickness of the crust by
47 the age of the substrate assuming constant growth (e.g., Barnes and Dymond, 1967).
48 Subsequently, absolute dating techniques were attempted using radioactive tracers, such
49 as U-Th series (younger than 750 ka; Ku, 1976) and $^{10}Be/^{9}Be$ (younger than 10 Ma;
50 Graham et al., 2004) dating.

51 For ferromanganese crusts older than 10 Ma, chronologies were established based
52 on empirical formulae on the Co flux into the ferromanganese crusts (e.g., Puteanus and
53 Halbach, 1988). However, these empirical formulae have not been well documented
54 theoretically, and Frank et al. (1999) found disagreement between the Co chronometer
55 and $^{10}Be/^{9}Be$ dating. Alternatively, $^{187}Os/^{188}Os$ chronology was successfully applied on a
56 ferromanganese crust by comparing its $^{187}Os/^{188}Os$ isotopic curve with the evolution of
57 $^{187}Os/^{188}Os$ in seawater established from sediments (Klemm et al., 2005). Although this
58 method has an advantage of covering long-term ranges back to 80 Ma, its low resolution
59 leads to considerable errors, to several million years.

60 Magnetostratigraphy could provide an alternative, independent dating technique
61 for ferromanganese crusts. Given the rate of geomagnetic reversals in the Cenozoic, a
62 successful magnetostratigraphy should provide more than one chronological control point
63 per million years. Once a magnetostratigraphic correlation is established, the accuracy of
64 the age model is secured by the astronomically calibrated magnetostratigraphic time scale
65 (1–40 k.y.; Lourens et al., 2004), which is not possible with the other geochemical
66 methods alone. Crecelius et al. (1973) pioneered the investigation of natural remanent
67 magnetization (NRM) in ferromanganese nodules and found evidence of geomagnetic
68 reversals. Paleomagnetic studies of thin (1–4 mm thick) slices of ferromanganese crusts

were performed by Chan et al. (1985) and Linkova and Ivanov (1993), but magnetostratigraphic correlations were not successful due to poor resolution of the paleomagnetic chrons.

The first apparently successful identification of paleomagnetic chrons in ferromanganese crusts was reported by Joshima and Usui (1998). They reported magnetostratigraphic correlations at 2.5 mm intervals from three ferromanganese crusts consistent with Co-based growth rates and radiochemical ages of substrate rocks. However, they found that the magnetostratigraphy-based growth rate for crust sample D96-m4 (16–17 mm/m.y.) was approximately three times higher than that based on $^{10}Be/^{9}Be$ ages (6 mm/m.y.; Usui et al., 2007), indicating that paleomagnetic chrons and/or subchrons were mismatched due to poor spatial resolution.

A spatial resolution finer than 1 mm is crucial to enable successful magnetostratigraphic correlations for slowly growing (1–10 mm/m.y.) ferromanganese crusts. However, preparation of specimens thinner than 1 mm from fragile crusts is not realistic. Thus, we developed an alternative method to construct age models for the crusts using a new high-resolution paleomagnetic method known as room-temperature scanning superconducting quantum interference device (SQUID) microscopy. Here we describe the results on thin sections of ferromanganese crust.

SAMPLE AND PREPARATION

Ferromanganese crust D96-m4 was selected from one of the three crust samples used by Joshima and Usui (1998). It was collected as an unoriented sample by dredging the Shotoku seamount (30°48.7′N, 138°19.14′E, water depth 1940 m) in the northwest Pacific Ocean during the R/V *Moana Wave* cruise MW9507 in June 1996. The seamount

92 is part of a currently inactive volcanic arc of Nishi-Shichito Ridge (Tamaki, 1985). A
93 basalt sampled from close to the location of D96-m4 has an $^{40}Ar/^{39}Ar$ plateau age of 9.0 ±
94 0.4 Ma (Ishizuka et al., 2003). The crust is 50 mm thick, is brownish-black, and in cross
95 section shows densely packed, weakly laminated growth patterns. The matrix consists of
96 vernadite as the major iron-manganese mineral, and minor quartz, plagioclase, smectite,
97 and apatite. The Mn/Fe ratio ranges from 0.78 to 1.01, and it contains <0.2% Cu, Ni, and
98 Co (Joshima and Usui, 1998).
99 A block of ferromanganese crust (Fig. 1A; left) was taken next to that studied by
100 Joshima and Usui (1998). Two slabs (length 35 mm, width 5 mm) were cut perpendicular
101 to the growth layers and perpendicular to each other, and polished thin sections of 0.2
102 mm thickness were made for scanning SQUID microscopy (MA1 and MB1 in Fig. 1A).
103 Next to these slabs, a columnar block was cut (15 mm × 20 mm; MC in Fig. 1A) and
104 sliced parallel to the growth lamination at 1.5 mm intervals using a 0.3-mm-thick
105 diamond-wire saw. The NRM and anhysteretic remanent magnetization (ARM) of the
106 slices were measured with a SQUID moment magnetometer.
107 **SQUID AND ELECTRON MICROSCOPY**
108 Scanning SQUID microscopy is a new tool for high-resolution mapping of
109 remanent magnetization in samples (Weiss et al., 2007). The instrument uses a
110 monolithic directly coupled niobium-based planar SQUID with a field sensitivity of
111 ~0.01 nT at a frequency of ~0.01 Hz (Baudenbacher et al., 2003; Fong et al., 2005; Weiss
112 et al., 2007). It measures the vertical component of the magnetic field above thin sections.
113 Measurements of the two thin sections MA1 and MB1 with the SQUID microscope were
114 taken inside a magnetic shield in planar grids with 85 μm spacing at a sensor-to-sample

distance (and approximate horizontal spatial resolution) of ~170 μm. Measurements were conducted for NRM before and after alternating field (AF) demagnetization at steps of 10, 20, 30, and 40 mT, and after giving the sample an ARM (direct current, DC field = 100 μT, alternating current field = 100 mT).

After SQUID microscopy, backscattered electron images (BEI) were obtained with an electron probe microanalyzer (EPMA, JEOL JXA-8900) at electron acceleration, probe current, and pixel sizes of 15 kV, 12 nA, and 2 μm, respectively. Compositional images (Si, Al, Ti, Mn, Fe, K, Mg, Ca, and P) were obtained by using the EPMA with a pixel size of 20 μm. On selected spots, major elements were examined with an electron probe diameter of 4 μm.

RESULTS

The NRMs of the slices (MC in Fig. 1A) are stable both for normal (Fig. 1B) and reversed (Fig. 1C) polarity intervals. An overprinting magnetization (probably viscous in origin) was removed after AF demagnetization at 10 mT. Declination and inclination (Figs. 1D and 1E; solid circles) are similar to those measured previously on the same crust (Joshima and Usui, 1998; gray circles in Figs. 1D and 1E). Although the polarity boundary observed at 5 mm depth can be recognized as the last geomagnetic reversal (0.78 Ma), earlier reversals are difficult to identify. The NRM intensity is lower for the older part of the crust (Fig. 1F); this is considered to be caused by multiple polarity transitions within each specimen, because ARM in the older part is higher than that of the younger part (Fig. 1G).

Figure 2 shows the results of the NRM magnetic field over thin-section MB1 imaged with the SQUID microscope together with BEI. Using an intensity scale of ±5

nT, magnetic stripes with downward (blue) and upward (red) orientation can be observed. The magnetic stripes are almost parallel to the growth pattern on the BEI (Fig. 2A). With an intensity scale of ±100 nT, intense positive and negative isolated spots can be observed. Some of these spots appear as pairs, indicating the presence of dipole magnetic sources. Opaque mineral grains in the center of some of the dipoles were identified by optical microscopy and their chemical composition determined with EPMA (see the following).

From the 24 thin slices used for magnetization measurements, 4 normal and 10 reversed-polarity stable magnetization directions were determined. Using these 14 directions, a mean direction was determined after inverting the reversed polarity directions of declination 233.7° and inclination 46.7° (with a 95% confidence circle of radius 6.5°). The positive inclination indicates that the ferromanganese crust was growing upward on the upper surface of the rock forming the seamount, although the crust was not oriented due to the sampling by a dredger.

After AF demagnetization, ARM was imparted upward perpendicularly to the surface of each thin section. Figure 2F shows that the magnetic field produced by ARM is dominantly upward with some intensity variation. The pattern does not directly correspond to the pattern of magnetic stripes observed for NRM. In Figure 2G (stretched intensity scale), there are tiny regions where a negative field (blue to light blue) is observed, indicating weakly ferromagnetic material. Strong negative fields (blue) in Figures 2E and 2F can be interpreted as magnetic dipoles originating from multidomain magnetic minerals not aligned to the DC bias field direction. Support for this interpretation is provided by the observation that the orientations of many of these

dipoles changed by tens of degrees or more between the NRM image and the AF 20 mT image. This instability indicates a low-coercivity source, which will be susceptible to ARM noise, as expected for multidomain grains.

The other weakly negative field (light blue) might represent the regions where magnetization is weak and the positive magnetization surrounding the region is producing the downward magnetic field. However, these regions are very small and most of the rest of the thin section is associated with a positive field. This confirms that the magnetic stripes are produced by upward and downward magnetization, and rules out the possibility that these are produced by the unidirectionally magnetized layers with magnetization intensity contrasts.

MAGNETIC MINERALS

Observations with the scanning electron microscope–EPMA revealed that the sources of strong NRM dipole fields before (Fig. 2C) and after (Fig. 2E) demagnetization consist of Fe oxides with sizes of a few tens of microns containing ~7% Ti with minor amounts of Al, Mn, and Mg (arrows in Fig. 2). Preliminary analysis of electron backscatter diffraction data indicates the presence of titanomagnetite of several microns, implying the presence of single domain (SD) and pseudo-single domain (PSD) grains. A thermomagnetic analysis on a magnetic extract revealed that Curie temperature is ~550 °C, which is consistent with titanomagnetite ($Fe_{3-z}Ti_zO_4$) with z = 7% (Dunlop and Özdemir, 1997), expected from EMPA analyses. These data collectively indicate that the major ferromagnetic mineral in our ferromanganese crust sample is titanomagnetite. The SEM-EPMA analyses indicate that the abundance of titanomagnetite is <<1%. In fact, magnetite and titanomagnetite are known accessory minerals in hydrogenetic

ferromanganese crusts (Bogdanova et al., 2008). The chemical composition of the titanomagnetite indicates a volcanogenic origin, implying that the NRM is predominantly a detrital remanent magnetization, although the possibility of a chemical origin cannot be ruled out.

ABSOLUTE AGE AND GROWTH RATE ESTIMATED BY MAGNETOSTRATIGRAPHY

We have chosen the magnetic image of NRM before demagnetization to identify the magnetic polarity boundaries because of the NRM's generally single component nature (as indicated by measurements of slices; Figs. 1B and 1C), and because further demagnetization did not enhance the magnetic stripes due to contamination of magnetic dipoles (Figs. 2C and 2F). We attempted to enhance the visibility of normal and reversed stripes with further data processing. First, we applied upward continuation (Blakely, 1996) of 200 μm (370 μm from surface of thin sections) on the original magnetic image to reduce the effect of magnetic dipoles, which have lower spatial resolution than the magnetic stripes.

Second, the following data processing was conducted to recognize the polarity boundaries for magnetostratigraphic correlation. Several tens of characteristic growth layer boundaries with significant contrast on BEIs were traced and registered as reference lines for the datum planes of simultaneous precipitation to be straightened. Mapping was conducted on the magnetic image parallel to the long axis with the previously registered reference lines (Figs. 3A and 3E). The lower boundary lines of the thin sections were used as base lines. From the straightened magnetic images, magnetic field values of –10 to +10 nT were extracted and summed perpendicularly to the growth axis within the

ferromanganese crust. Magnetic field values >10 nT were neglected because these are considered as noise mostly originating from randomly oriented dipole sources. Finally, the zero crossings were extracted as magnetostratigraphic boundaries and correlated with the standard magnetostratigraphic time scale of Lourens et al. (2004). The angle of the growth layers and the lines perpendicular to the baseline changes from 0° to 38°, implying a maximum distortion of the time scale by no more than 27%.

Figure 3 illustrates the results of data processing on MA1 and MB1 and their magnetostratigraphic correlations. Both MA1 (Fig. 3A) and MB1 (Fig. 3E) show magnetic stripes parallel to the surface of the ferromanganese crust after the above corrections. Most of the zero crossings (Figs. 3B and 3D) were correlated with the standard magnetostratigraphic time scale (Lourens et al. 2004; Fig. 3C). Correlations were primarily made based on the long polarity chrons, including Brunhes normal and Matuyama reversed chrons. The extracted polarity boundary depths were plotted versus ages (Fig. 3F). Growth rates are estimated to be 4.99 ± 0.43 and 4.90 ± 0.32 mm/m.y. (errors are in 2σ) for the upper (0–3.596 Ma; blue solid line) and lower (4.631–7.212 Ma; blue broken line) parts of MA1. Between 3.596 and 4.641 Ma, the growth rate is apparently slower (3.20 ± 2.84 mm/m.y.); this can be interpreted as a result of change in the tilt angle observed on the BEI. We calculated the average growth rate for MA1 to be 4.95 ± 0.27 mm/m.y. The growth rate for MB1 can be calculated as 5.25 ± 0.37 mm/m.y. (red line). The growth rate for D96-m4 based on magnetostratigraphy can be calculated as 5.10 ± 0.23 mm/m.y. by averaging MA1 and MB1.

Usui et al. (2007) obtained a growth rate of ~6 mm/m.y. for the ferromanganese crust D96-m4 by $^{10}Be/^{9}Be$ using a ^{10}Be half-life of 1.5 m.y. Recently, a sequence of

carefully designed laboratory experiments led to the best estimate for the ^{10}Be half-life of 1.387 ± 0.012 m.y. (Chmeleff et al., 2010). Applying this new half-life to the data of Usui et al. (2007) and excluding the oldest points, we obtain a growth rate of 6.04 ± 0.18 mm/m.y. The ^{10}Be/^{9}Be initial value ($1.29 \pm 0.05 \times 10^{-7}$) is consistent with a modern ^{10}Be/^{9}Be ratio for the studied area ($1.36 \pm 0.05 \times 10^{-7}$; Usui et al., 2007), which suggests that the youngest paleomagnetic chron is the Brunhes normal polarity chron. The growth rate from magnetostratigraphy is ~16% lower than that from ^{10}Be/^{9}Be dating. Considering the meandering growth structure (change in tilt of layers along sampling baseline), the errors due to half-life, violation of the constancy of production and preservation of ^{10}Be, thickness (a few millimeters) of ^{10}Be analysis, and identification of polarity boundaries, the new dating method with the SQUID microscope shows great promise for absolute chronological control.

CONCLUSIONS

We have shown that ultrafine-scale magnetostratigraphy using state of the art SQUID microscopy is a promising chronological tool for determining absolute ages and growth rates for the ferromanganese crusts. Approximately oppositely magnetized stripes oriented parallel to bedding were clearly observed on thin sections of a crust and could be correlated with the standard magnetostratigraphic time scale. The average growth rate obtained by magnetostratigraphy (5.1 ± 0.2 mm/m.y.) is within 16% of that independently estimated by ^{10}Be/^{9}Be (6.0 ± 0.2 mm/m.y.). SQUID micromagnetostratigraphy in combination with other chronometric techniques is thus a potentially powerful technique for high-resolution absolute chronology of ferromanganese crusts. In ideal cases, the method may provide an alternative quick dating

tool for the ferromanganese crust without laborious chemical separation and mass spectroscopy, once the routine analysis is established. The method can also serve as a valuable tool for calibrating other chronological data and can be used to test the accuracy of experimentally derived half-lives of radioactive isotopes such as ^{10}Be in ferromanganese crusts.

ACKNOWLEDGMENTS

We thank the scientific staff and crew of R/V *Moana Wave* Cruise MW9507, A. Owada for technical assistance in preparing polished sections for SQUID microscopy, and Jérôme Gattacceca and two anonymous reviewers for helpful comments on the manuscript. Oda was supported by a Grant-in-Aid for Scientific Research from the Japan Society for the Promotion of Science (21654071). Weiss was supported by the U.S. National Science Foundation Collaboration in Mathematical Geosciences Program.

REFERENCES CITED

Banakar, V.K., Galy, A., Sukumaran, N.P., Parthiban, G., and Volvaiker, A.Y., 2003, Himalayan sedimentary pulses recorded by silicate detritus within a ferromanganese crust from the Central Indian Ocean: Earth and Planetary Science Letters, v. 205, p. 337–348, doi: 10.1016/S0012-821X(02)01062-2.

Barnes, S.S., and Dymond, J.R., 1967, Rates of accumulation of ferromanganese nodules: Nature, v. 213, p. 1218–1219, doi: 10.1038/2131218a0.

Baudenbacher, F., Fong, L.E., Holzer, J.R., and Radparvar, M., 2003, Monolithic low-transition-temperature superconducting magnetometers for high resolution imaging

magnetic fields of room temperature samples: Applied Physics Letters, v. 82, p. 3487–3489, doi: 10.1063/1.1572968.

Blakely, R.J., 1996, Potential theory in gravity and magnetic applications: New York, Cambridge University Press, 441 p.

Bogdanova, O.Y., Gorshkov, A.I., Novikov, G.V., and Bogdanov, Y.A., 2008, Mineralogy of morphogenetic types of ferromanganese deposits in the world ocean: Geology of Ore Deposits, v. 50, p. 462–469, doi: 10.1134/S1075701508060044.

Chan, L.S., Chu, C.L., and Ku, T.L., 1985, Magnetic stratigraphy observed in ferromanganese crust: Royal Astronomical Society Geophysical Journal, v. 80, p. 715–723.

Chmeleff, J., von Blanckenburg, F., Kossert, K., and Jakob, D., 2010, Determination of the ^{10}Be half-life by multicollector ICP-MS and liquid scintillation counting: Nuclear Instruments and Methods in Physics Research, section B, v. 268, p. 192–199, doi: 10.1016/j.nimb.2009.09.012.

Crecelius, E.A., Carpenta, R., and Merrill, R.T., 1973, Magnetism and magnetic reversals in ferromanganese nodules: Earth and Planetary Science Letters, v. 17, p. 391–396, doi: 10.1016/0012-821X(73)90206-9.

Dunlop, D., and Özdemir, O., 1997, Rock magnetism: Fundamentals and frontiers: New York, Cambridge University Press, 573 p.

Fong, L.E., Holzer, J.R., McBride, K.K., Lima, E.A., and Baudenbacher, F., 2005, High-resolution room-temperature sample scanning superconducting quantum interference device microscope configurable for geological and biomagnetic applications: Review of Scientific Instruments, v. 76, 053703, doi: 10.1063/1.1884025.

298 Frank, M., O'Nions, R.K., Hein, J.R., and Banakar, V.K., 1999, 60 Myr records of major
299 elements and Pb-Nd isotopes from hydrogenous ferromanganese crusts:
300 Reconstruction of seawater paleochemistry: Geochimica et Cosmochimica Acta,
301 v. 63, p. 1689–1708, doi: 10.1016/S0016-7037(99)00079-4.
302 Graham, I.J., Carter, R.M., Ditchburn, R.G., and Zondervan, A., 2004,
303 Chronostratigraphy of ODP 181, Site 1121 sediment core (Southwest Pacific Ocean),
304 using $^{10}Be/^{9}Be$ dating of entrapped ferromanganese nodule: Marine Geology, v. 205,
305 p. 227–247, doi: 10.1016/S0025-3227(04)00025-8.
306 Ishizuka, O., Uto, K., and Yuasa, M., 2003, Volcanic history of the back-arc region of the
307 Izu-Bonin (Ogasawara) arc, *in* Larter, R.D., and Leat, P.T., eds., Intra-oceanic
308 subduction systems: Tectonic and magmatic processes: Geological Society of
309 London Special Publication 219, p. 187–205, doi: 10.1144/GSL.SP.2003.219.01.09.
310 Joshima, M., and Usui, A., 1998, Magnetostratigraphy of hydrogenetic manganese crusts
311 from northwestern Pacific seamounts: Marine Geology, v. 146, p. 53–62, doi:
312 10.1016/S0025-3227(97)00131-X.
313 Klemm, V., Levasseur, S., Frank, M., Hein, J.R., and Halliday, A.N., 2005, Osmium
314 isotope stratigraphy of a marine ferromanganese crust: Earth and Planetary Science
315 Letters, v. 238, p. 42–48, doi: 10.1016/j.epsl.2005.07.016.
316 Ku, T.L., 1976, The uranium-series methods of age determination: Annual Review of
317 Earth and Planetary Sciences, v. 4, p. 347–379, doi:
318 10.1146/annurev.ea.04.050176.002023.
319 Linkova, T.I., and Ivanov, Y.Y., 1993, Magnetic stratigraphy in ferromanganese crusts
320 from Central Pacific: Geology of the Pacific Ocean, v. 9, p. 187–197.

Lourens, L.J., Hilgen, F.J., Laskar, J., Shackleton, N.J., and Wilson, D., 2004, The Neogene Period, *in* Gradstein, F.M., et al., eds., A geologic time scale 2004: Cambridge, Cambridge University Press, p. 409–440.

Prasad, M.S., 1994, Australasian microtektites in a substrate: A new constraint on ferromanganese crust accumulation rates: Marine Geology, v. 116, p. 259–266, doi: 10.1016/0025-3227(94)90045-0.

Puteanus, D., and Halbach, P., 1988, Correlation of Co concentration and growth rate—A method for age determination of ferromanganese crusts: Chemical Geology, v. 69, p. 73–85, doi: 10.1016/0009-2541(88)90159-3.

Tamaki, K., 1985, Two modes of back-arc spreading: Geology, v. 13, p. 475–478, doi: 10.1130/0091-7613(1985)13<475:TMOBS>2.0.CO;2.

Usui, A., Graham, I.J., Ditchburn, R.G., Zondervan, A., Shibasaki, H., and Hishida, H., 2007, Growth history and formation environments of ferromanganese deposits on the Philippine Sea Plate, northwest Pacific Ocean: The Island Arc, v. 16, p. 420–430, doi: 10.1111/j.1440-1738.2007.00592.x.

van de Flierdt, T., Frank, M., Halliday, A.N., Hein, J.R., Hattendorf, B., Günther, D., and Kubik, P.W., 2004, Deep and bottom water export from the Southern Ocean to the Pacific over the past 38 million years: Paleoceanography, v. 19, p. 1–14, doi: 10.1029/2003PA000923.

Weiss, B.P., Lima, E.A., Fong, L.E., and Baudenbacher, F.J., 2007, Paleomagnetic analysis using SQUID microscopy: Journal of Geophysical Research, v. 112, B09105, doi: 10.1029/2007JB004940.

FIGURE CAPTIONS

Figure 1. A: Backscattered electron images of thin sections (MA1 and MB1) and photo of columnar block (MC) used for bulk measurements from block of crust D96-m4 (left). MA1 and MB1 were taken with parallel growth pictures on their surface and perpendicular to each other; MA1 (MB1) with surface facing +X (+Y) axis. Marks on scale of columnar block (MC) are specimen boundaries. Typical vector end-point diagrams of bulk paleomagnetic measurements on thin sliced specimens are plotted. B: Normal (depth = 1.5 mm) polarity intervals. NRM—natural remanent magnetization. C: Reversed (depth = 8.3 mm) polarity intervals. Solid circles (open circles) denote magnetization vector at each demagnetization steps projected onto horizontal (vertical) plane. Numbers denote demagnetization steps (in mT). D: Declination after alternating field (AF) demagnetization at 20 mT. E: Inclination after AF demagnetization at 20 mT. F: Intensity of NRM before demagnetization. G: Intensity of anhysteretic remanent (ARM) magnetization plotted versus corrected depth (solid circles). Thin sliced specimens were cut parallel to growth layer. Corrected depth is depth collected for dip angle (32°) of MC. Declination and inclination (in D, E; measured by Joshima and Usui, 1998) after 10 mT alternating field demagnetization are also plotted as gray circles and lines. **[[SU: what is "Div." in Figs. B, C? Need space around mult ×, = signs]]**

Figure 2. Analysis of thin-section MB1. A: Backscattered electron image (BEI). B: Natural remanent magnetization (NRM) before demagnetization with scale of ±5 nT. C: With scale of ±100 nT. D: NRM after 20 mT alternating field demagnetization with scale of ±5 nT. E: With scale of ±100 nT. F: Anhysteretic remanent magnetization (ARM) with scale of ±100 nT. G: With scale of ±5 nT. Thin black lines in B–G indicate outer rim of

crust. Arrows indicate spots where titanomagnetite grains were observed with electron probe microanalyzer. **[[SU: on right axis, need space before mT]]**

Figure 3. Magnetostratigraphic correlations using SQUID (see text) microscope maps of undemagnetized natural remanent magnetization for thin-sections MA1 and MB1. Magnetic images were straightened using backscattered electron image growth pattern. A, E: After upward continuation of 200 μm for MA1 and MB1, respectively. B, D: Stacked for MA1 and MB1, respectively. C: Stacks were correlated with standard magnetostratigraphic time scale (Lourens et al., 2004). F: Depths were plotted versus age for MA1 (blue circles) and MB1 (red circles). Black circles are $^{10}Be/^{9}Be$ data (Usui et al., 2007). Growth rates estimated for each method are shown as inset (see text for details). **[[SU: don't see any "inset" in figure?]]**

Figure1
Click here to download Figure: Fig.1.pdf

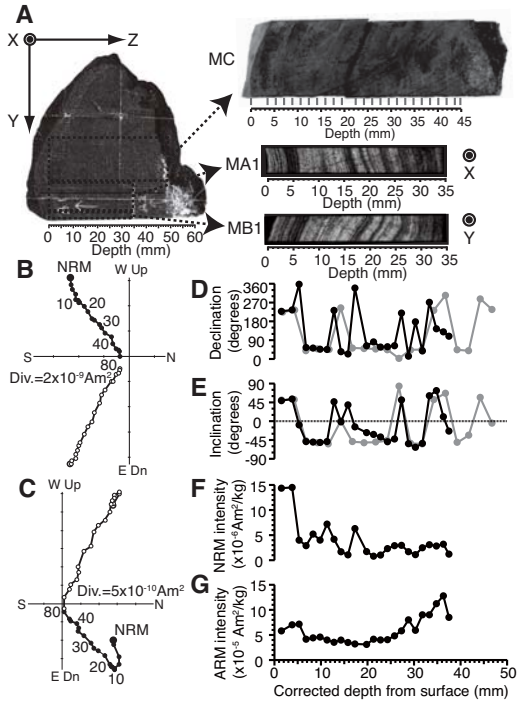

Hirokuni ODA Figure 1 Fig.1.ai

Figure2
Click here to download Figure: Fig.2.pdf

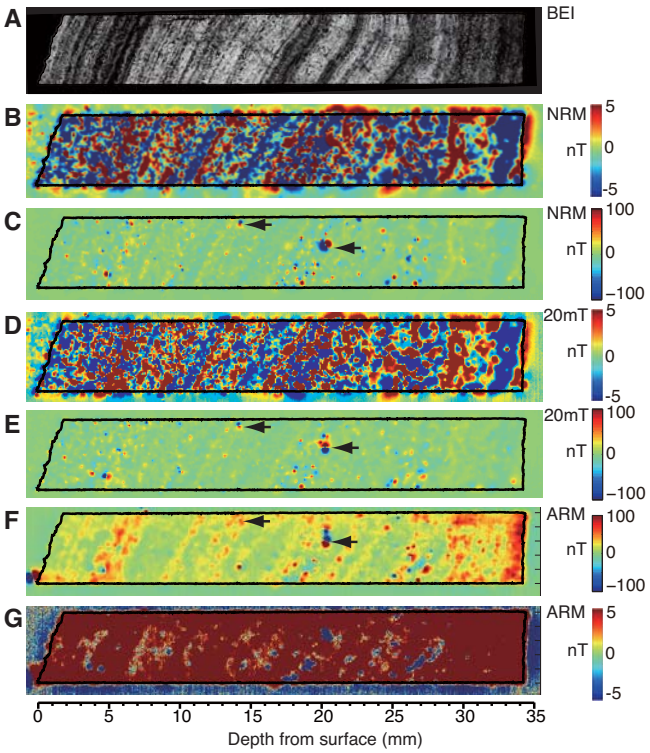

Hirokuni ODA Figure 2. Fig.2.ai

Figure3
Click here to download Figure: Fig.3.pdf

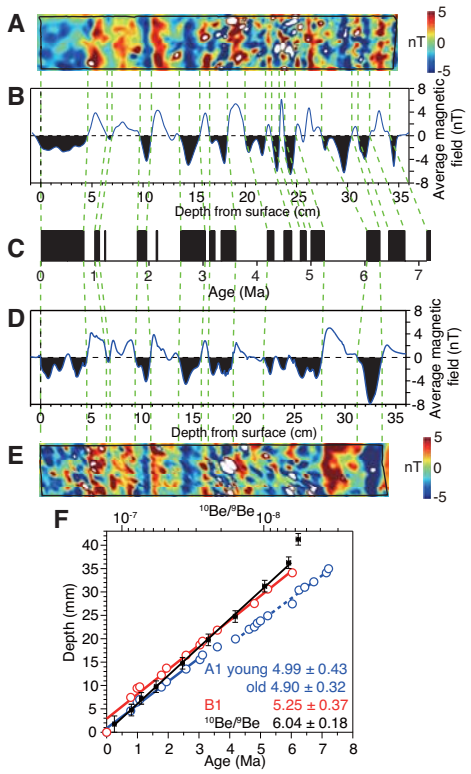

Hirokuni ODA Figure 3. Fig.3.ai